Carbon 110 (2016) 8–16

Contents lists available at ScienceDirect

Carbon

journal homepage: www.elsevier.com/locate/carbon

Electromechanical, self-sensing and viscoelastic behavior of carbon fiber tows

Miguel Ramirez, D.D.L. Chung*

Composite Materials Research Laboratory, Department of Mechanical and Aerospace Engineering, University at Buffalo, State University of New York, Buffalo, NY 14260-4400, USA

ARTICLE INFO

Article history:
Received 27 February 2016
Received in revised form
2 August 2016
Accepted 31 August 2016
Available online 31 August 2016

ABSTRACT

The electromechanical, electrical-resistance-based self-sensing and viscoelastic stress-relaxation phenomena of unsized binderless pitch-based carbon fiber tows have been observed for the first time, using the elastica loop test innovatively modified with four-probe tow electrical resistance measurement. The resistance increases upon fiber breakage and decreases upon stress-relaxation-related fiber rearrangement. With a fixed tensile strain applied, the resistance decreases with time, levelling off after ~40 s, due to the relative movement of the fibers causing more fiber-fiber contact as the tow relaxes, and indicating viscoelastic stress-relaxation behavior. Minor fiber fracture and inelastic behavior occur more upon loading than unloading. Strain-controlled fatigue loading results in cycle-by-cycle monotonically increasing fraction of fibers broken. Loop major-to-minor axis ratio increase accompanies fiber fracture, which promotes the inelastic behavior. The increase of the fraction of fibers broken upon strain cycling becomes more abrupt when this fraction exceeds 40% and the ratio exceeds 1.4. This fraction increases monotonically with progressively increasing strain amplitude, being gradual at fraction <4% and significant at fraction >4%, with tow failure occurring upon loading from an effectively unloaded state with fraction 22%. For fatigue loading at a relatively high strain amplitude, tow failure occurs upon loading from an effectively unloaded state with fraction 81%.

1. Introduction

Carbon fibers are commonly fabricated and used in the form of tows [1,2] rather than single fibers. A tow is a collection of a large number of aligned fibers in the absence of a binder. Tows of fibers can be woven to form a fabric or braided to form a tube. Tows can be suitably oriented and infiltrated with a resin or matrix precursor in order to form a polymer-matrix composite material. Ideally, the resin or matrix precursor spatially surrounds each fiber in the tow. However, such perfect complete infiltration does not necessarily occur, especially when the resin or matrix precursor is of high viscosity, thus resulting in matrix voids within the fiber tow. In spite of the practical importance of tows, relatively little research has been conducted on them. Most research has been conducted on either a single fiber or fiber composites.

The ability of a material to sense its own condition is known as self-sensing [3]. Self-sensing may be used to monitor a process in which the material is being manufactured, thus enabling real-time control of the manufacturing conditions (i.e., smart manufacturing). Furthermore, self-sensing materials may also be used for monitoring its structural health or other conditions of the material as it is being used. Structural health monitoring is particularly important for strategic or aging structures, such as aircraft. Monitoring is commonly achieved by the use of sensors that are attached to or embedded in the material to be monitored. Examples of sensors include optical fibers, piezoelectric sensors and resistive strain gages. However, monitoring involving the attachment or embedment of sensors suffers from the high cost and low durability of the sensors. In the case of embedded sensors, an additional issue relates to the loss of the mechanical properties of the material because of the intrusive nature of the embedment. On the other hand, self-sensing does not have these disadvantages.

Due to the electrical conductivity of carbon fibers and the non-conductivity of the polymer matrix that embeds the fibers, the electrical resistivity of a carbon fiber polymer-matrix composite is sensitive to the fiber arrangement, interface microstructure and

* Corresponding author.
E-mail address: ddlchung@buffalo.edu (D.D.L. Chung).
URL: http://alum.mit.edu/www/ddlchung

http://dx.doi.org/10.1016/j.carbon.2016.08.095
0008-6223/

imperfections in the composite, thereby providing electromechanical effects that enable electrical resistance measurement to be effective for the self-sensing of the strain and damage in carbon fiber polymer-matrix composites [3–6]. On the other hand, the electrical resistivity of a single carbon fiber essentially does not change prior to the brittle failure of the fiber [7], because the fiber arrangement does not pertain to a single fiber and the strain of a carbon fiber is small prior to failure. As a consequence, electrical resistance measurement is essentially insensitive to the strain or non-fracture damage of a fiber, though it is obviously sensitive to the fracture of a fiber. This paper provides the first report of the electromechanical and associated self-sensing behavior of carbon fiber tows. The self-sensing reported here pertains to the sensing of fiber fracture and is based on electrical resistance measurement. Hence, this work enables a carbon fiber tow to be a sensor of its own condition.

In general, the mechanical properties of a material can include elastic and viscous aspects. A material that exhibits both elastic and viscous characters is said to be viscoelastic. Viscoelastic materials are most commonly polymers with long linear molecules, which allow various types of intramolecular and intermolecular movement. The movement enables the material to undergo bulk viscoelastic deformation. Recent work concerning exfoliated graphite [8,9] has shown that viscoelastic behavior can stem from friction-related interfacial movement rather than bulk deformation.

The viscous behavior is a time-dependent phenomenon that is associated with a lag of the stress response to an applied strain or equivalently the lag of the strain response to an applied stress. In contrast, there is no such lag response for a purely elastic material. An example of a viscoelastic effect is stress relaxation, which refers to the gradual decrease in the stress under a constant strain, thereby relieving the state of stress. Stress relaxation commonly occurs in polymers, due to the movement of the macromolecules in a polymer. For example, it has been reported for carbon fiber polymer-matrix composites [10,11]. It has also been reported in carbon fiber (without a matrix) during high-temperature graphitization [12]. However, it has not been previously reported in carbon materials at ordinary temperatures in the absence of a matrix material.

Complete understanding of the mechanical behavior of a viscoelastic material must involve consideration of both the viscous character and the elastic character. The viscous aspect of mechanical behavior is practically important for mechanical energy dissipation, which relates to vibration damping and sound absorption. Vibration damping is needed for aircraft, cars, wind turbines, bridges, railroad, tall buildings, helmets, etc. Sound absorption is needed for railroad, highways, aircraft, wind turbines, etc.

Materials with a high elastic modulus tend to be weak in the viscous behavior, so their mechanical properties are dominated by the elastic behavior. Carbons and ceramics are examples of materials that typically exhibit high elastic modulus. In contrast, polymers such as rubber tend to have substantial viscous behavior, due to the movement of the macromolecules in them. Thus, carbon materials such as single carbon fibers are essentially purely elastic. However, strong viscous character has recently been reported for exfoliated graphite [8], due to the friction-related relative movement of the cell walls of the exfoliated graphite [9]. This paper gives the first report of the viscoelastic stress-relaxation behavior of carbon fiber tows in the absence of a matrix. This behavior stems from the friction-related relative movement of the fibers in the tow [13,14].

The elastica loop test [15–19] is a purely mechanical test that is conventionally used to test the mechanical properties of a fiber tow. As the radius of curvature of the loop decreases, the stress and strain at the tip of the loop increase. In spite of the historic use of the loop test, electrical resistance measurement during loop testing has not been previously reported. Due to the sensitivity of the tow's resistivity to fiber fracture, by measuring the resistance during loop testing with loading and subsequent unloading at various strain amplitudes and during fatigue loading, this work shows the effectiveness of the tow to provide electrical-resistance-based self-sensing of the degree of fiber fracture in the tow.

Fiber tows in the form of loops are involved in weaving, braiding and stitching [20]. In particular, stitching is conducted using yarns in the through-thickness direction in order to provide a three-dimensional carbon fiber preform.

Because of the sensitivity of the resistance to the rearrangement of the fibers in the tow and the occurrence of fiber rearrangement during stress relaxation, resistance measurement also allows study of the tow's viscoelastic stress-relaxation behavior. Moreover, due to the feasibility of real-time resistance measurement, the time dependence associated with the viscoelastic behavior can be studied by resistance measurement.

The objectives of this work are (i) to observe the electromechanical behavior of carbon fiber tows, (ii) to investigate the effectiveness of carbon fiber tows for electrical-resistance-based self-sensing, (iii) to observe and study the viscoelastic behavior of carbon fiber tows, and (iv) to extend the loop test to include electrical resistance measurement during the test.

2. Experimental methods

A tow of continuous carbon fibers is subjected to a four-probe electrical resistance measurement. In addition, the measurement is conducted during loop testing with strain-controlled loading and subsequent unloading at various strain amplitudes (i.e., at various minor axis values of the loop resulting from the loaded and effectively unloaded states). While the loop test is subjected to a four-probe electrical measurement, the strain remains constant. Silver paint in conjunction with fine copper wire wrapped around the tow is used for the electrical contacts on the tow.

The carbon fibers are Amoco Thornel P-100, mesophase-pitch-based, unsized, without twist, with 10-μm diameters, tensile modulus 724 GPa [21], with measured electrical resistivity of 1.8×10^{-4} Ω cm for a single fiber. The number of fibers in a tow approximately ranges from 400 to 700. This number is determined for each tow studied by electrical resistance measurement, with the number calculated based on the simple equation for resistors in parallel, using the measured value of the resistivity of a single fiber in the calculation.

The four-probe method is used for measuring the electrical resistance of the tow while the tow is in the form of a loop. The voltage contacts (B and C in Fig. 1) are at the regions located outside the loop with a separation distance ranging from 110 to 170 mm, as separately measured for each specimen. The current contacts (A and D in Fig. 1) are further away from the voltage contacts toward the ends of the tow. A known current of 5.00 mA is applied through the current contacts using a Keithley 224 power source. The potential difference between the voltage contacts is measured using a Keithley 2002 precision multimeter in conjunction with LabView data-acquisition software. During a resistance measurement, no part of the loop is allowed to touch another part of the loop. The tow resistance is in the range from 4 to 10 Ω. Resistance measurement is conducted at particular values of the minor axis, rather than being conducted continuously during change in the minor axis. Current is constantly applied to the specimen even during the change from one strain level to another. Because the resistance decreases with time from the start of imposing a particular strain level and then levels off (a phenomenon first observed in this work and presented in Sec. 3.3), the resistance for a particular state is

obtained after the levelling off. While one end of the loop (the left end in Fig. 1) is held fixed, the minor axis dimension is adjusted to a pre-determined value by manual pulling of the tow from the free end (the right end in Fig. 1). For each of the loaded and effectively unloaded states, the dimensions of the major and minor axes are measured using digital calipers.

The effectively unloaded state does not mean a state of zero load. Rather it means the initial state of low load. In testing a given specimen, the first measurement is at this effectively unloaded state, followed by a loaded state. Measurements are alternately conducted for the effectively unloaded and loaded states. The measurement number refers to the number of the consecutive measurements in chronological order, with the odd numbers referring to effectively unloaded states and the even numbers referring to loaded states.

The minor axis dimension is used to calculate the strain present on the fiber tow while placed in a loop. The strain ε is given by

$$\varepsilon = \frac{1.07d}{D}$$

where d is the diameter of a single fiber (10 μm, according to the manufacturer) and D is the minor axis of the loop [15]. The stress on the fiber tow is calculated as the product of the modulus and the strain; this is valid when the deformation is purely elastic.

3. Results and discussion

3.1. During progressive increase of the strain amplitude

3.1.1. Tow with 394 ± 5 fibers

Fig. 2(a) shows the resistance measured at successive effectively unloaded state and loaded state corresponding to progressively increasing strain amplitudes. A high strain amplitude is obtained by having a large difference between the minor axis value of the loaded state and that of the effectively unloaded state. The tow has 394 ± 5 fibers.

Fig. 2(b) shows the corresponding strain and stress values calculated based on the minor axis and the single fiber modulus respectively. The strain of the loaded state increases from 0.0004 to 0.0015 as the strain amplitude increases in the regime of minor damage (the regime of slight resistance increase, Fig. 2(a)) and increases from 0.0015 to 0.0033 in the regime of major damage (the regime of abrupt resistance increase, Fig. 2(a)). The strain of the effectively unloaded state is about 0.0004 for all the strain amplitudes. The elongation at break of the single carbon fiber is 0.0031 [21]. The observed strain of 0.0033 at the failure of the tow is close to this value. The stress of the loaded state is up to 2.38 GPa, which is near the tensile strength of the single fiber [21]. The stress of the effectively unloaded state is about 0.29 GPa.

The resistance increases gradually with decreasing minor axis from 26 to 5 mm due to minor damage (Fig. 2(c)), with 3% of the fibers being broken, (based on calculation using the measured resistance and the equation for resistors in parallel, with a broken fiber being considered as an open circuit) and increases abruptly with further decrease of the minor axis below 5 mm due to major damage (Fig. 2(d); with 8% of the fibers being broken, again based on calculation using the measured resistance).

Extensive damage (Fig. 2(e), with 18% of the fibers broken (based on calculation using the measured resistance) occurs upon loading to a minor axis of 3 mm. Subsequent unloading to a minor axis of 26 mm gives additional damage (Fig. 2(f), with the two voltage contacts shown), so that the fraction of fibers broken is 20%, based on calculation using the measured resistance. Still subsequent loading to a minor axis of 2 mm causes immediate complete failure (with essentially 100% of the fibers broken), so that the resistance abruptly rises to a value that is too large to be measured. There is rough consistency between the fraction of fibers broken based on calculation and that based on visual observation.

Fig. 2(g) shows the evolution of the fraction of fibers broken as the strain amplitude increases. The fraction increases gradually from 0% to 3% upon both loading and unloading in the regime of

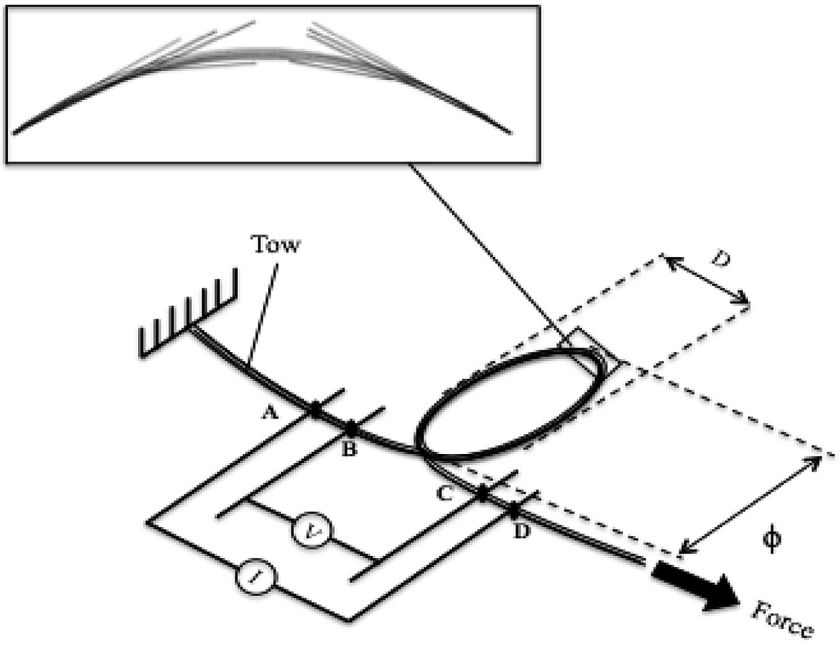

Fig. 1. Schematic illustration of the elastic loop test that has been modified by inclusion of electrical resistance measurement. The resistance measurement involves four electrical contacts, i.e., A, B, C and D. The inset shows the part of the tow near the tip of the tow loop. Fiber fracture occurs in this region, though not all of the fibers fracture. The ends of the tow away from the loop are fixed on two different pieces of writing paper by using adhesive tape. The strain-controlled loading on the tow is applied via manual translation of one of the two pieces of paper.

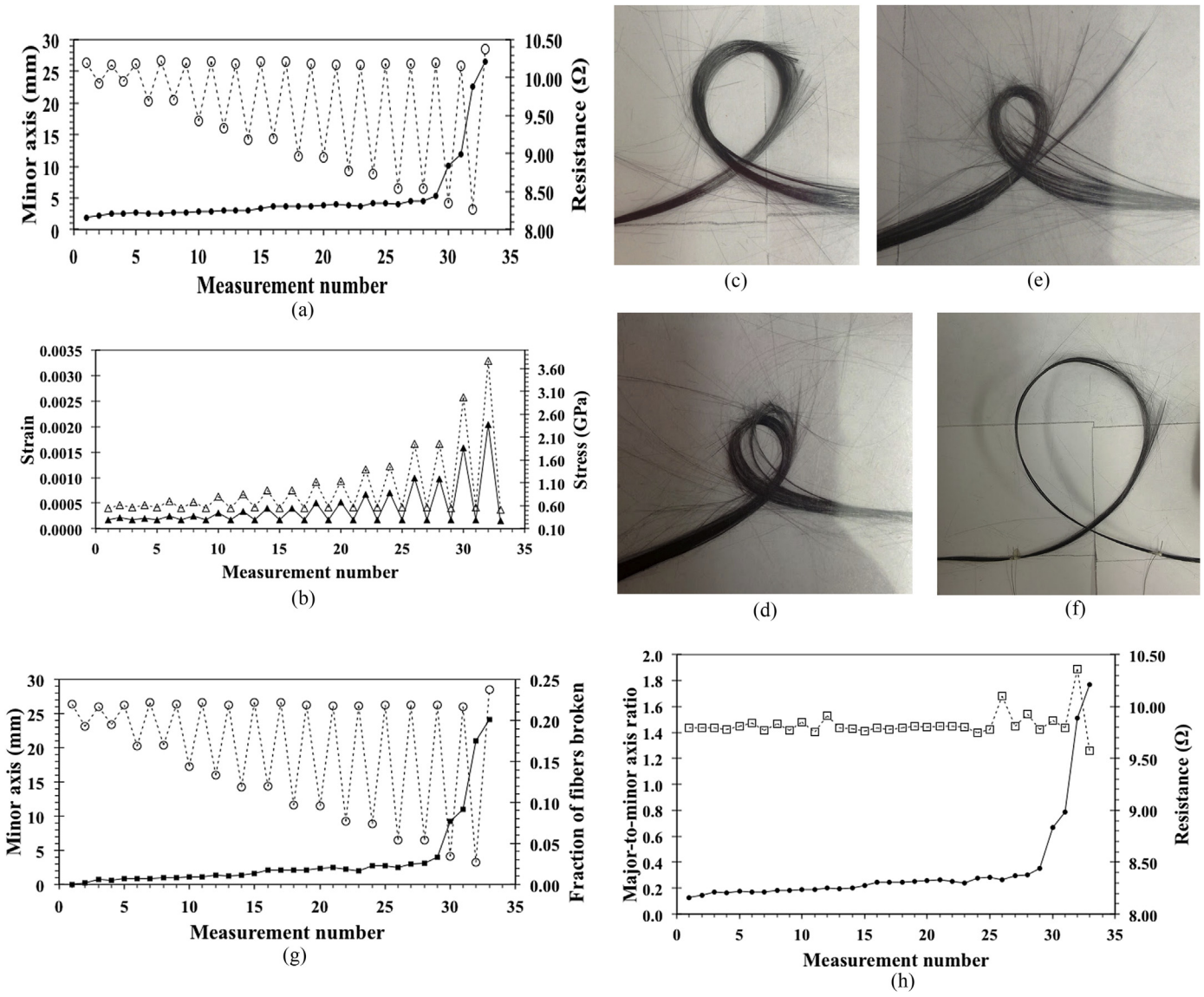

Fig. 2. Effect of progressively increasing strain amplitude on the electrical resistance for a tow with 394 ± 5 fibers. (a) Minor axis (○) and resistance (●), each vs. the measurement number. (b) Strain (Δ) and stress (▲), each vs. the measurement number, as obtained by calculation based on the minor axis dimension, assuming the absence of viscous behavior. (c) Photo taken at measurement 26, loaded state, with 3% fibers broken. (d) Photo taken at measurement number 30, loaded state, with 8% fibers broken. (e) Photo taken at measurement number 32, loaded state, with 18% fibers broken, immediately prior to the effectively unloaded state of Fig. 2(a). (f) Photo taken a measurement number 33, effectively unloaded state, with 20% fibers broken, immediately prior to the loading that causes failure. (g) Fraction of fibers broken (■) and minor axis (○), each vs. the measurement number. (h) Major-to-minor axis ratio (□) and resistance (●), each vs. the measurement number. (A colour version of this figure can be viewed online.)

minor damage, which extends up to the minor axis of 7 mm in the loaded state. At higher strain amplitudes, the fraction of fibers broken increases abruptly from 3% to 20%, with failure occurring during loading after the last effectively unloaded state with 20% of the fibers broken.

The transition from the regime of minor damage to the regime of major damage occurs at the effectively unloaded state with 3% of the fibers broken (Fig. 2(g)). The immediately subsequent loading marks the clear start of the major damage regime; this is associated with a strain of 0.0026 and a stress of 1.86 GPa (Fig. 2(b)).

Fig. 2(h) is the corresponding plot that shows the ratio of the major-to-minor axis of the loop. A ratio of 1.34 is conventionally considered to be the maximum value for purely elastic behavior of the fibers [16]. Fig. 2(h) shows a ratio value of 1.40, which is above 1.34, indicating a minor deviation from elasticity. Even though the individual fibers are purely elastic, the inter-fiber movement in the tow can give rise to a degree of viscous behavior. This ratio essentially does not change throughout the increases in strain amplitude, except, in the regime of major damage, the ratio is higher for the loaded state than the immediately prior effectively unloaded state.

3.1.2. *Tow with 647 ± 5 fibers*

Fig. 3 gives corresponding results for a tow with 647 ± 5 fibers. As in Figs. 2(a) and 3(a) shows that the transition from the minor damage regime to the major damage regime occurs at a minor axis of 5 mm.

Fig. 3(b) shows that the strain of the loaded state ranges from 0.0005 to 0.0035. The strain value of 0.0035 is close to but above 0.0031, which is the elongation at failure for a single fiber [21]. For the effectively unloaded state, the strain is about 0.0005. The stress of the loaded state is up to 2.5 GPa. Failure occurs after loading at 2.4 GPa, which is near the single-fiber tensile strength of 2.2 GPa

[21]. That the tensile strength is apparently exceeded is not real and is attributed to the stress-induced spreading of the fibers in a tow resulting in imprecise measurement of the minor axis value. The stress of the effectively unloaded state is about 0.35 GPa.

In the loaded state with minor axis at 5 mm, 4% of the fibers are broken, based on calculation using the resistance (Fig. 3(c)). In the effectively unloaded state with minor axis 21 mm, 5% of the fibers are broken, based on calculation using the resistance (Fig. 3(d)). In the effectively unloaded state with minor axis 18 mm, 20% of the fibers are broken, based on calculation using the resistance (Fig. 3(e)). Subsequent loading to a minor axis of 3 mm causes immediate complete failure (with essentially 100% of the fibers broken), so that the resistance abruptly rises to a value that is too large to be measured. There is approximate agreement between the fraction of fibers broken based on calculation and that based on visual observation.

As shown in the optical photos in Fig. 3(c), (d) and 3(e), fiber breakage occurs at the outer side of the loop, which experiences the greatest degree of tension. Fiber breakage essentially does not occur at the inner side of the loop. This means that the fibers break under tension. Compression plays a minor role, if any.

The tensile strength of the fiber is higher than the compressive strength, but the tensile ductility is expected to be lower than the compressive ductility. Since the experiment is conducted under displacement control rather than load control, the ability to withstand a given displacement rather than the ability to withstand a given stress governs the fracture tendency, thus resulting in the fiber breakage occurring at the tension side of the tow.

Fig. 3(f) shows that the fraction of fibers broken increases gradually with increasing strain amplitude upon both loading and unloading in the regime of minor damage, which is up to a strain amplitude corresponding to the minor axis being 6 mm in the loaded state. Subsequent increase in the strain amplitude causes abrupt increase in the fraction of fibers broken upon both loading and unloading, until failure occurs during the last loading, which occurs after the effectively unloaded state with 24% of the fibers broken.

The transition from the regime of minor damage to the regime of major damage occurs at the effectively unloaded state with 5% of the fibers broken (Fig. 3(f)). The immediately subsequent loading marks the clear start of the major damage regime; this is associated with a strain of 0.0035 and a stress of 2.4 GPa (Fig. 3(b)).

Fig. 3(g) shows the corresponding plot that shows the major-to-minor axis ratio of the loop. This ratio is again 1.40 and does not show any systematic change as the strain amplitude progressively increases, except that, in the regime of major damage, it increases up to 1.95 and is higher for the loaded state than the immediately prior effectively unloaded state. As the major-to-minor axis ratio increases, the probability of fiber breakage also increases. It has been previously reported that this ratio increases from 1.34 up to 1.57 as the strain increases [16]. The increase observed in this work from 1.40 to 1.95 indicates that the viscous behavior increases as the extent of major damage increases.

3.1.3. Comparison of the results of the two tows

In spite of the difference in the number of fibers in the tow in Secs. 3.1.1 and 3.1.2, Figs. 2 and 3 give qualitatively similar results. For the tow with 394 ± 5 fibers, failure occurs upon loading after the effectively unloaded state with 20% fibers broken, such that the immediately prior loaded state has strain 0.0033 and stress 2.4 GPa. For the tow with 647 ± 5 fibers, failure occurs upon loading after the effectively unloaded state with 24% fibers broken, such that the immediately prior loaded state has strain 0.0034 and stress 2.4 GPa. This means that the failure characteristics are similar for the two tows. However, the characteristics for the change from the minor damage regime to the major damage regime are different between the two tows. For the tow with 394 ± 5 fibers, this change occurs at the effectively unloaded state with 3% fibers broken, such that the immediately subsequent loaded state has strain 0.0025 and stress 1.8 GPa. However, for the tow with 647 ± 5 fibers, this change occurs at the effectively unloaded state with 5% fibers broken, such that the immediately subsequent loaded state has strain 0.0035 and stress 2.4 GPa. This difference between the two tows is attributed to the difference in the progressive loading conditions (as shown by comparing Figs. 2(b) and 3(b)) rather than the difference in the number of fibers in the tow. That the number of fibers in a tow essentially does not affect the inter-tow friction has been previously reported [14].

3.2. During fatigue loading

This work includes testing under fatigue loading, with the resistance and minor axis dimension measured at alternating effectively unloaded and loaded states for a constant strain amplitude (Fig. 4(a)). The tow contains 502 ± 5 fibers.

As the minor axis varies between 26 and 11 mm for each cycle (corresponding to a strain amplitude in the regime of minor damage, Fig. 2(a)), the resistance increases monotonically cycle by cycle. Commencing with the first cycle, the fractional change in resistance per cycle is 0.45% on the average, due to minor fatigue damage. Upon increase of the constant strain amplitude so that the minor axis varies between 26 and 8 mm in each cycle (corresponding to a strain amplitude in the regime of minor damage, Fig. 2(a)), the average fractional change in resistance per cycle is greater (3.3%).

Upon further increase of the constant strain amplitude so that the minor axis varies between 26 and 4 mm (corresponding to a strain amplitude that is in the regime of minor damage, but close to the regime of major damage, Fig. 2(a)), the average fractional change in resistance per cycle (with a cycle including loading and unloading) is 5.6% in the regime of minor fatigue damage (up to measurement number 25). Major fatigue damage starts at measurement number 25 and causes the fractional change in resistance per cycle to increase abruptly up to 58%, which is the value just before failure (Fig. 4(a)).

Fig. 4(b) shows that the strain of the loaded state ranges from 0.0026 to 0.0046 and the stress of the loaded state ranges from 1.9 to 3.3 GPa. The data for measurement numbers 24 and 26 have been omitted due to an error in the minor axis measurement. For the initial effectively unloaded state, the strain is 0.0003 and the stress is 0.2 GPa. The last loaded state prior to failure upon subsequent loading has a stress of 2.6 GPa (close to the single-fiber tensile strength of 2.2 GPa [21]) and a strain of 0.0036 (close to the single-fiber elongation at failure of 0.0031 [21]).

At measurement number 32 in the loaded state, 29% of the fibers are broken, based on calculation using the resistance (Fig. 4(c)). At measurement number 33 in the effectively unloaded state, 81% of the fibers are broken with stress reaching approximately 0.31 GPa towards failure (Fig. 4(d)). Moreover, upon loading after measurement number 33, failure occurs and the resistance abruptly increases to a value that is too high to be measured (denoting an open circuit). The change from the minor fatigue damage regime to the major fatigue damage regime occurs at a resistance of 10 Ω, which corresponds to 43% of the fibers being broken, based on calculation using the resistance. There is approximate consistency between the fraction of fibers broken based on calculation and that based on visual observation.

Fig. 4(e) shows that the fraction of fibers broken increases with load cycling, starting from almost the start of the cycling. This fraction steadily increases as cycling progresses, such that it increases more significantly in the last 5 cycles prior to failure, i.e.,

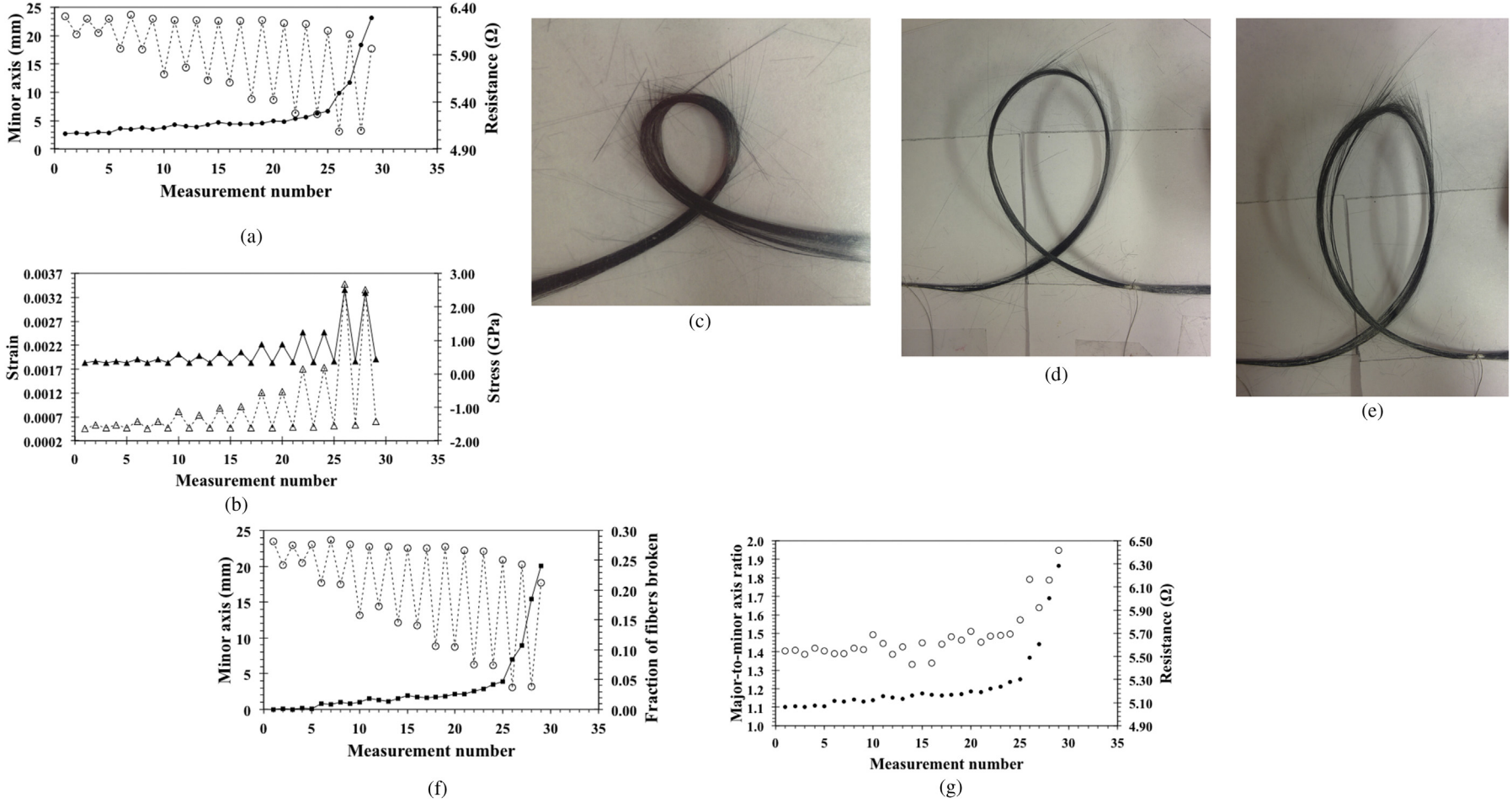

Fig. 3. Effect of progressively increasing strain amplitude on the electrical resistance for a tow with 647 ± 5 fibers. (a) Minor axis (○) and resistance (□), each vs. the measurement number. (b) Strain (Δ) and stress (▲), each vs. the measurement number. (c) Photo taken at measurement number 22, loaded state, with 4% fibers broken. (d) Photo taken at measurement number 25, effectively unloaded state, with 5% fibers broken. (e) Photo taken at measurement number 29, effectively unloaded state, with 20% fibers broken. (f) Fraction of fibers broken (■) and minor axis (○), each vs. the measurement number. (g) Major-to-minor axis ratio (○) and resistance (●), each vs. the measurement number. (A colour version of this figure can be viewed online.)

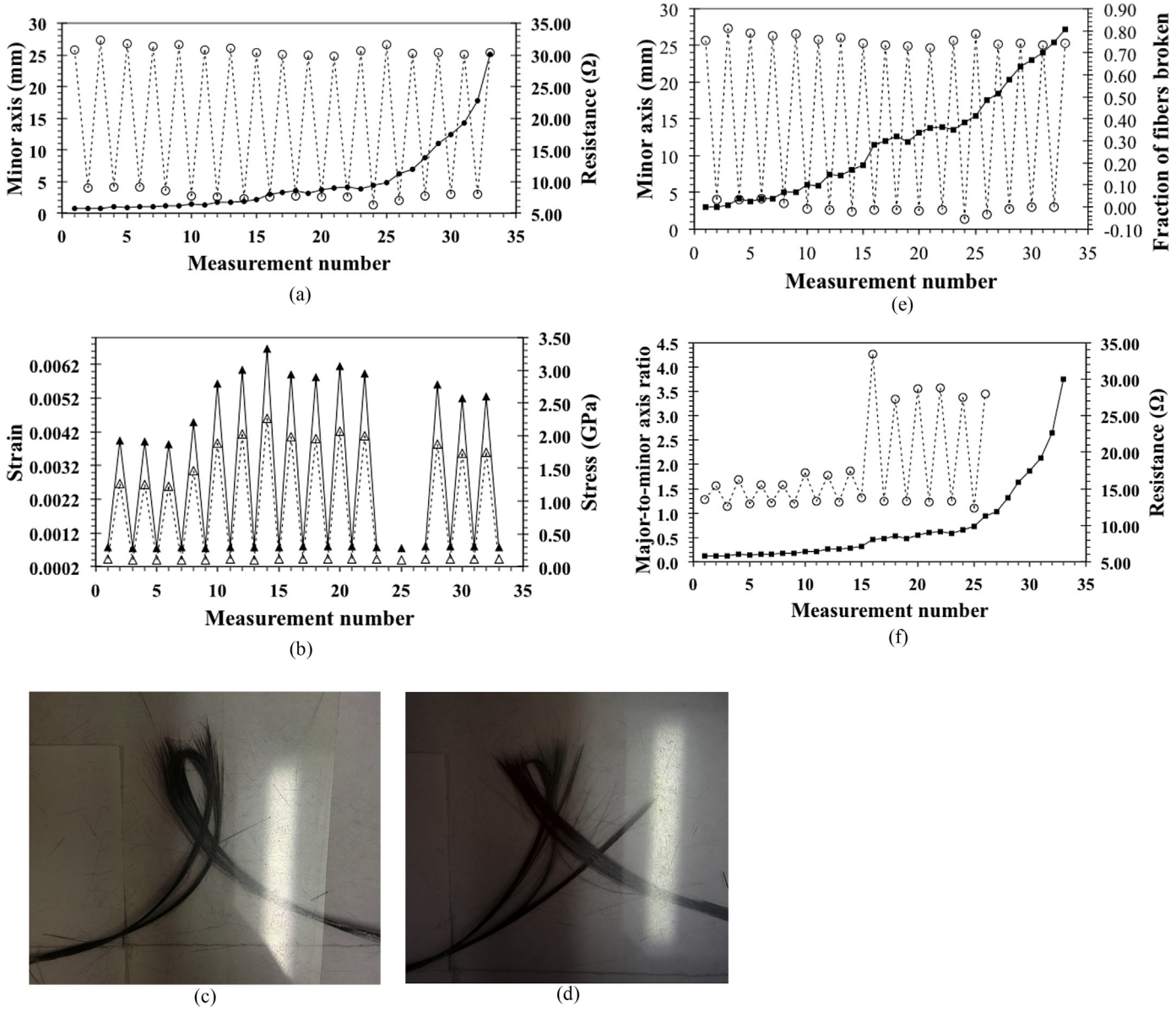

Fig. 4. Effect of fatigue loading. (a) Minor axis (○) and resistance (●), each vs. the measurement number. (b) Strain (△) and stress (▲), each vs. the measurement number. The data points at measurement number 24 and 26 are not shown, because they are unreasonably high and judged to be incorrect. (c) Photo taken at measurement number 32, loaded state, with 29% fibers broken. (d) Photo taken at measurement number 33, effectively unloaded state, with 81% fibers broken. (e) Minor axis (○) and fraction of fibers broken (■), each vs. the measurement number. (f) Major-to-minor axis ratio (○) and resistance (■), each vs. the measurement number. The values of the major-to-minor axis ratio are not shown for the data obtained close to failure, due to the large data scatter of these data points. (A colour version of this figure can be viewed online.)

when the fraction of fibers broken exceeds about 40%. The fraction of fibers broken tends to increase more upon loading than upon unloading, such that the difference between the loading and unloading effects is clear in the regime of minor damage. In the regime of major damage, the fraction of fibers broken increases upon both loading and unloading. This means that, in the regime of minor damage, damage is inflicted mainly during loading, but, in the regime of major damage, damage is inflicted both during loading and unloading.

The fraction of fibers broken immediately before the loading that gives the final failure is 20% for the case of loading at progressively increasing strain amplitudes (Figs. 2 and 3), but is 81% for the case of fatigue loading at a fixed high strain amplitude (Fig. 4(d)). This implies that fatigue loading at fixed high strain amplitude is more abusive to the tow than loading at progressively increasing strain amplitudes.

Fig. 4(f) shows that the major-to-minor axis ratio is higher in the loaded state than the immediately prior effectively unloaded state or the subsequent effectively unloaded state. The ratio for the loaded state tends to increase upon load cycling, while the ratio for the effectively unloaded state essentially does not change upon cycling. Fig. 4(f) and (e) indicate that both the ratio and the fraction of fibers broken increase more during loading than unloading. These observations mean that fiber fracture is associated with an increase in the ratio.

The combination of Fig. 4(f) and (e) indicates that a relatively high major-to-minor axis ratio tends to correlate with a relatively high fraction of fibers broken and that the increase in the major-to-minor axis ratio with load cycling and the increase in the fraction of fibers broken with load cycling are both significant when the fraction of fibers broken exceeds 40%, which corresponds to the major-to-minor axis ratio exceeding 1.40. This ratio consistently

reaches values as high as 3.6. This high value of the ratio indicates significant deviation from elasticity. This means that viscous character becomes substantial when the fraction of fibers broken exceeds 40%.

3.3. Time dependence

This section addresses the time dependence of the resistance from the time of the start of applying a certain strain. The tow contains 670 ± 5 fibers. At a fixed strain, the resistance decreases with time from the starting time for a particular strain, as consistently observed in repeated testing for various values of the fixed strain. Upon application of a given fixed strain (minor axis), the resistance decreases with time, with the rate of resistance decrease diminishing with increasing time, such that the decrease tends to level off after 35–45 s (Fig. 5). Although Fig. 5 shows two representative curves, similar resistance decrease with time occurs for all the strain levels used in this work, whether under progressively increasing strain amplitudes or under fatigue loading at a fixed strain amplitude.

Since the current is constantly applied even during the change from one strain level to another, the observed resistance decrease at a given fixed strain is not due to the resistance (Joule) heating of the tow. The constant current does not allow the tow to cool down, however small is the extent of resistance heating. If the observed resistance decrease were due to the resistance heating of the tow and not due to viscoelasticity, the resistance decrease would not have changed from a levelled-off characteristic immediately before the change in strain to a decreasing resistance characteristic immediately after the change in strain.

The observed resistance decrease cannot be due to electric polarization, which would have increased the measured resistance rather than decreasing it. Carbon fibers are a conductive material rather than a dielectric material, so that polarization should be negligible anyway. Electric polarization has been reported in carbon fiber (short) cement-matrix composites, which derive their dielectric behavior from the cement matrix [22].

The major-to-minor axis ratio is 1.60 at the start of the loaded state and is 1.40 at the start of the subsequent effectively unloaded state. That the ratio is higher for the loaded state than the subsequent effectively unloaded state is consistent with the results in Fig. 4(f). As shown in Sec. 3.2, fiber fracture would cause this ratio to increase. Both values of 1.60 and 1.40 are above 1.34 [14], indicating a degree of deviation from purely elastic behavior. This suggests that the viscous character is stronger in the loaded state than the effectively unloaded state.

Fiber fracture would have caused the resistance to increase abruptly. Thus, the observed time-dependent resistance decrease cannot be due to fiber fracture. Rather, it is attributed to the slight rearrangement of the fibers in the tow (i.e., inter-fiber movement) as stress relaxation occurs at a fixed strain. The fiber rearrangement is such that the degree of fiber-fiber contact increases. Fiber-fiber contact decreases the tow resistance because the contacts allow detouring of the current from one fiber to an adjacent one, so that imperfections in the fibers will not increase the tow resistance as much as the case of no fiber-fiber contact. Stress relaxation is commonly exhibited by polymers due to the molecular movement in the polymer. It is a viscoelastic effect.

The observed resistance decrease with time is small - up to 0.2% in Fig. 5(a). The small fractional change is expected, as the resistance change is just due to a subtle change in the fiber arrangement in the tow as the tow relaxes.

The decrease in resistance with time is similar for the various strain levels and for the loaded and effectively unloaded states. This similarity is consistent with the prior report that the inter-tow friction is essentially independent of the load or the loading direction [14]. On the other hand, the resistance decrease is monotonic for the loaded state (Fig. 5(a)) than the effectively unloaded state (Fig. 5(b)), because the loaded state is obtained upon the application of stress, which increases the degree of fiber alignment, whereas the return from the loaded state to the effectively unloaded state has a squishing effect on the tow and the squishing is accompanied by the buckling of the fibers, thereby messing up the fiber arrangement in the tow. The messing up would cause irregularities in the curve of resistance vs. time as the messed-up structure relaxes. The fact that the compressive strength of the fibers (0.5 GPa) is much smaller than the tensile strength (2.2 GPa) [21] is consistent with the notion of messing up the fiber arrangement upon compression.

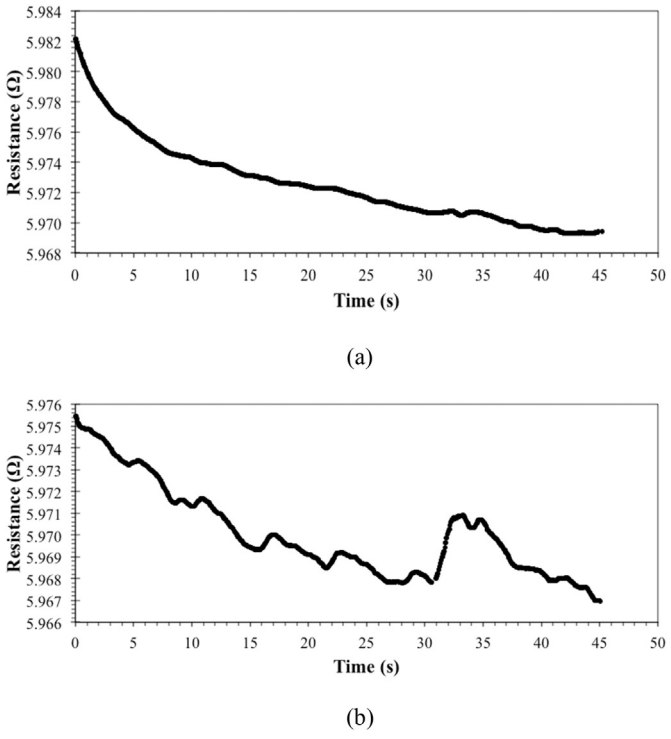

Fig. 5. Time-dependence of the resistance. (a) Resistance vs time from the start (time = 0) of attaining the loaded state with minor axis 13.41 mm and major-to-minor axis ratio 1.60. (b) Resistance vs. time from the start (time = 0) of having returned to the effectively unloaded state with minor axis 24.13 mm and major-to-minor axis ratio 1.40, with the effectively unloaded state occurring immediately after the loaded state in (a).

The viscoelastic behavior of rubber stems from the movement of the molecules in the rubber. However, the viscoelastic behavior in a carbon fiber tow stems from the movement of the fibers relative to one another. This movement occurs at the interface between the fibers. Such interfacial-friction-related mechanism of viscoelastic behavior is to be distinguished from the conventional bulk viscoelastic deformation mechanism (as in the case of rubber). The interfacial mechanism has been previously reported in exfoliated graphite, which derives its strong viscoelastic behavior from the friction-related movement between the cell walls of the exfoliated graphite [8,9].

In general, viscoelastic polymeric materials such as rubber suffer from the inability of these materials to withstand high temperatures or harsh chemical environments, in addition to the strong temperature dependence of their viscoelastic behavior. In contrast, the interfacial mechanism, as in the case of a carbon fiber tow, does not suffer from these issues.

4. Practical relevance

The technique of this paper may be applied to various types of carbon fiber. However, fibers that are less brittle than the P-100 fiber do not break as easily and, as a result, the technique may not give results that are as rich as those reported in this paper.

The technique of this paper can be extended from DC to AC. Under DC condition, only the resistance is measured. Under AC condition, both resistance and capacitance are measured, in addition to the frequency dependence of each quantity. Thus, the signature corresponding to a given degree of damage of the tow is much richer under AC than DC. Therefore, the extension from DC to AC is expected to increase the versatility and sensitivity of this technique.

This paper addresses the loop in the absence of a matrix, as is relevant to the use of a tow in weaving, braiding or stitching. In particular, through-thickness stitching (known as z-stitching) is used in the preparation of three-dimensional carbon fiber preforms for the fabrication of carbon-carbon composites and carbon fiber ceramic-matrix composites.

This work can be extended to the case of the tow having been infiltrated with a resin prior to curing or after different degrees of curing, as is relevant to composite fabrication by filament winding. Furthermore, the study can be extended to the case of the tow having been infiltrated with a resin, which is subsequently completely cured, as is relevant to pultruded composite structures such as fishing poles, which undergo bending during use.

The practical implementation of the technique of this paper may be facilitated by wireless measurement of the resistance. The wireless method is in contrast to the measurement with wires reported in this paper.

5. Conclusion

This work provides the first observation of the electromechanical and viscoelastic stress-relaxation behavior of carbon fiber tows. The electromechanical behavior enables electrical-resistance-based self-sensing. Furthermore, the conventional elastica loop test, a purely mechanical test, has been extended innovatively in this work to include electrical resistance measurement. The resistance of the tow loop, with a broken fiber being considered as an open circuit, provides a reasonable estimate of the fraction of fibers broken. The fracture of some of the fibers in the tow tends to occur upon strain-controlled loading/unloading in the regime of major damage, but it tends to occur more upon loading than unloading in the regime of minor damage. The loop's major-to-minor axis ratio also tends to be higher upon loading than unloading and is promoted by fiber fracture.

The fraction of fibers broken increases monotonically with increasing strain amplitude, such that it increases gradually in the regime of minor damage (with less than about 4% of the fibers broken, corresponding to strain less than 0.003 and stress less than about 2.1 GPa) and increases abruptly in the subsequent regime of major damage.

For the case of progressively increasing strain amplitude, failure of the tow occurs upon loading from the effectively unloaded state that is characterized by having about 22% of the fibers broken, and, for the immediately prior loaded state, having strain 0.0033 and stress about 2.3 GPa. For the case of fatigue loading at a relatively high strain amplitude, failure of the tow occurs upon loading from the effectively unloaded state that is characterized by having 81% of the fiber broken.

Fatigue loading of the tow results in monotonic increase of the fraction of fibers broken cycle by cycle, starting from essentially the start of the load cycling, such that fiber fracture tends to occur more during loading and unloading. The increase of the fraction of fibers broken upon cycling becomes more abrupt when this fraction exceeds 40% and when the major-to-minor axis ratio exceeds 1.4. The fractional change in resistance per cycle is 5.6% on the average in the minor-damage regime that occurs prior to the abrupt resistance increase; it increases abruptly up to 58%, which is the value just before tow failure.

Upon application of a fixed strain, the resistance decreases with time, with the rate of resistance decrease diminishing with increasing time, such that the decrease tends to level off after about 40 s. This decrease in resistance is a viscoelastic stress-relaxation effect that is due to friction-related relative movement of the fibers as the tow relaxes at the fixed strain.

Acknowledgement

The authors are grateful to the C-STEP Program of the State University of New York at Albany for the partial support of this work.

References

[1] W. Li, Z. Chen, J. Li, X. Chen, H. Xuan, X. Wang, Preparation of PAN/phenolic-based carbon/carbon composites with flexible towpreg carbon fiber, Mater. Sci. Eng. A A485 (1–2) (2008) 481–486.
[2] S. Stenard, Mechanical characterization & design architecture of graphite T 700 12K/epoxy wide tow triaxial braided composites, Int. SAMPE Symp. Exhib. 47 (2002) 1471–1487.
[3] D.D.L. Chung, Carbon materials for structural self-sensing, electromagnetic shielding and thermal interfacing, Carbon 50 (2012) 3342–3353.
[4] D.D.L. Chung, Damage detection using self-sensing concepts, J. Aerosp. Eng. 221 (G4) (2007) 509–520.
[5] D. Wang, D.D.L. Chung, Through-thickness piezoresistivity in a carbon fiber polymer-matrix structural composite for electrical-resistance-based through-thickness strain sensing, Carbon 60 (1) (2013) 129–138.
[6] X. Wang, D.D.L. Chung, Piezoresistive behavior of carbon fiber in epoxy, Carbon 35 (10/11) (1997) 1649–1651.
[7] X. Wang, D.D.L. Chung, Electromechanical behavior of carbon fiber, Carbon 35 (5) (1997) 706–709.
[8] D.D.L. Chung, Interface-derived extraordinary viscous behavior of exfoliated graphite, Carbon 68 (2014) 646–652.
[9] L. Xiao, D.D.L. Chung, Mechanical energy dissipation modeling of exfoliated graphite based on interfacial friction theory, Carbon 108 (2016) 291–302.
[10] Y. Masuko, M. Kawai, Application of a phenomenological viscoplasticity model to the stress relaxation behavior of unidirectional and angle-ply CFRP laminates at high temperature, Compos. Part A Appl. Sci. Manuf. 35A (7–8) (2004) 817–826.
[11] J.C. Thesken, C.L. Bowman, S.M. Arnold, R.C. Thompson, Time-Temperature Dependent Response of Filament Wound Composites for Flywheel Rotors, ASTM Special Technical Publication, 2003, pp. 55–74 stp 1436(Composite materials: testing and design, fourteenth volume).
[12] D. Li, C. Lu, G. Wu, Y. Yang, Z. Feng, X. Li, F. An, Zhang Bao. Heat-induced internal strain relaxation and its effect on the microstructure of polyacrylonitrile-based carbon fiber, J. Mater. Sci. Technol. (Shenyang, China) 30 (10) (2014) 1051–1058.
[13] B. Cornelissen, M.B. de Rooij, B. Rietman, R. Akkerman, Frictional behavior of carbon fiber tows: a contact mechanics model of tow-tow friction, Text. Res. J. 84 (14) (2014) 1476–1488.
[14] N.D. Chakladar, P. Mandal, P. Potluri, Effects of inter-tow angle and tow size on carbon fibre friction, Compos. Part A 65 (2014) 115–124.
[15] H.M. Hawthorne, On non-Hookean behavior of carbon fibers in bending, J. Mater. Sci. 28 (9) (1993) 2531–2535.
[16] M. Furuyama, M. Higuhi, K. Kubomura, H. Sunago, H. Jiang, S. Kumar, Compressive properties of single-filament carbon fibers, J. Mater. Sci. 28 (6) (1993) 1611–1616.
[17] T. Hashishin, H. Kohara, H. Iwanaga, S. Takeuchi, Fracture behavior of alumina and carbon fibers in the loop test, J. Ceram. Soc. Jpn. 110 (1284) (2002) 772–774.
[18] M. Glowania, S. Schneiders, J. Hesselbach, K. Simonis, T. Gries, Knot- and loop tensile tests of ultra high-modulus pitch-based carbon fibers, J. Text. Eng. 19 (85) (2012) 10–14.
[19] I. Krucinska, S. Krucinski, Numerical investigation of intrinsic mechanical properties of carbon fibers, Text. Res. J 67 (5) (1997) 316–320.
[20] W. Kuo, The role of loops in 3D fabric composites, Compos Sci. Technol. 60 (2000) 1835–1849.
[21] C.T. Ho, D.D.L. Chung, Bromination of graphitic pitch based carbon fibers, Carbon 28 (6) (1990) 831–837.
[22] S. Wen, D.D.L. Chung, Electric polarization in carbon fiber reinforced cement, Cem. Concr. Res. 31 (2) (2001) 141–147.